n-Type doping of ε-Ga2O3 epilayers by high-temperature tin diffusion

n-Type Doping of ε-Ga_2O_3 Epilayers by High-Temperature Tin Diffusion

Alessio Bosio[1], Antonella Parisini[1], Alessio Lamperti[2], Carmine Borelli[1], Laura Fornasini[1], Matteo Bosi[3], Ildikò Cora[4], Zsolt Fogarassy[4], Béla Pécz[4], Zsolt Zolnai[4], Attila Németh[5], Salvatore Vantaggio[1] and Roberto Fornari[1,3]

[1] *University of Parma, Department of Mathematical, Physical and Computer Sciences, Viale delle Scienze 7/A, 43124 Parma, Italy*

[2] *Institute for Microelectronics and Microsystems, (CNR-IMM) Agrate Unit, Via Camillo Olivetti 2, 20864 Agrate Brianza (MB), Italy*

[3] *Institute of Materials for Electronics and Magnetism (CNR- IMEM), Viale delle Scienze 37/A, 43124 Parma, Italy*

[4] *Centre for Energy Research, Institute of Technical Physics and Materials Science, Konkoly-Thege M. út 29-33., Budapest, 1121 Hungary*

[5] *Wigner Research Centre for Physics, Institute for Particle and Nuclear Physics, Konkoly-Thege M. út 29-33, H-1121 Budapest, Hungary*

Abstract: The good control of the *n*-type doping is a key issue for the fabrication of efficient devices based on ε-Ga_2O_3 epilayers. In this work we studied the possibility of doping the ε-Ga_2O_3 thin films, epitaxially grown on *c*-oriented sapphire by metal-organic chemical vapor deposition, by means of a post-deposition treatment. For the first time, the *n*-type doping was achieved by depositing a tin-rich SnO_2 film on top of the ε-Ga_2O_3 layer and keeping this bi-layer system for 4 hours at a temperature of 600 °C in an evacuated furnace. The diffusion of Sn atoms into the ε-Ga_2O_3 film is evidenced by time-of-flight secondary-ion mass spectrometry depth profiles. Room-temperature resistivity of the order of 1 Ω·cm is obtained and the electrical characterization revealed a conduction mechanism based on variable range hopping, according to the Mott's model.

Keywords: ε-Ga_2O_3, Sn-doping, Diffusion, ToF-SIMS, RBS, Electrical characterization

1. Introduction

Among semiconductors characterized by a very wide energy gap, Ga_2O_3 has long been studied for its interesting electro-optical properties [1, 2]. This semiconductor can be synthesized in different polytypes (α, β, γ and ε) [3], however most devices have been made so far with the thermodynamically stable β phase. For different applications, a good control on charge carrier concentrations is essential. Some of them require low (solar-blind detectors) [4], intermediate (field effect transistors) [5] and high conductivity (power electronics) [6]. The ability to extrinsically dope this material depends on the opportunity of incorporating elements with adequately small ionization energy and to contemporarily suppress the formation of compensating defects [7]. For the β-phase, O-vacancies were estimated to act as deep donor centers [8], and also cation vacancies show a natural tendency to become compensating defects [9], while interstitial atoms play a minimal role [10]. The balance between donor and compensating states is ultimately established by thermodynamic defect equilibrium [11]. Similar considerations were also put forward for other Ga_2O_3 polymorphs [12].

Elements of the IVb group of the periodic table are natural candidates as donor defects in Ga_2O_3, when substitutional to Ga cations.

Indeed, it has been demonstrated that Si, Ge and Sn are effective *n*-type dopants in β-Ga_2O_3, reaching concentrations (N_D-N_A) over 10^{19} cm^{-3}, at room temperature (RT), with different growth

techniques [13, 14, 15]. In this case, the transport of the charge carriers involves delocalized states giving rise to a metallic-like conduction mechanism [16].
In literature, very little information concerning the doping of ε-Ga_2O_3, and related charge transport mechanism, is available. In a previous work, [17] it was shown that *n*-type ε-Ga_2O_3 epilayers could be grown by metal-organic chemical vapor deposition (MOCVD), by adding silane directly into the growth chamber. A maximum RT value of the net electron concentration (N_D-N_A) of about 10^{18} cm^{-3} was obtained, with mobility values of the order of few $cm^2/V{\cdot}s$. These reduced values of the charge carrier mobility are not due to a poor crystalline quality of the ε-Ga_2O_3 epilayers, but rather to the transport mechanism, which is based on hopping between localized states in the energy gap. In this case, the conduction occurs through the variable range hopping transport mechanism described by the Mott's model.
In this work a novel route to *n*-type doping of ε-Ga_2O_3 epilayers, through high temperature post-growth treatment, is presented for the first time. This process is based on the thermally-activated diffusion of Sn atoms into undoped ε-Ga_2O_3 films, giving rise to a RT net doping concentration in the range (10^{17}÷10^{18}) cm^{-3}, corresponding to a RT - resistivity of about (1÷10) Ω·cm. Through time-of-flight secondary-ion mass spectrometry (ToF-SIMS) measurements we demonstrate that Sn atoms actually penetrate into the ε-Ga_2O_3 crystal lattice and the electrical characterization shows a conduction mechanism very similar to that described for Si doping.

2. Experimental

The nominally-undoped ε-Ga_2O_3 thin films were epitaxially grown by MOCVD on 2-inch c-oriented sapphire substrates. Details on the growth conditions are reported in [18].
Before any additional treatment, in order to produce a standard surface conditions for all samples, the ε-Ga_2O_3 films were etched in a solution of hydrofluoric (50%) and nitric acid (50%) - (the so-called F-N acid) for 1 min and then sequentially rinsed in acetone, isopropanol, deionized water and finally blown in dry nitrogen. Immediately after this pre-treatment, the ε-Ga_2O_3 samples were loaded into an evacuated sputtering chamber for the deposition of a Sn-containing material. The deposition started when a limit pressure of 10^{-4} Pa was reached. The idea was to cover the surface of the ε-Ga_2O_3 film with a Sn-based material and then annealing this bi-layer at high temperature, exploiting the thermally-activated diffusion of the Sn atoms into the ε-Ga_2O_3 layer. The diffusion process must be carried out at a temperature sufficiently high to promote the Sn diffusion but anyway well below the phase-transition temperature [19]. We have thus fixed the anneal temperature at 600 °C. Considering the low melting point of Sn (231.9 °C), the use of a pure metallic film of tin is not possible as it would fully melt and produce separated droplets on the semiconductor, owing to surface tension of the liquid. To overcome this drawback, a tin-rich oxide film was deposited on top of the ε-Ga_2O_3 in order to provide a reservoir for the high-temperature diffusion of Sn atoms. The oxide film was deposited by using a 13.56 MHz radio-frequency (r.f.) magnetron reactive sputtering, applying a r.f. power density of about 0.7 W/cm^2 over a 3-inch Sn-target. The process gas was Ar with a pressure of 0.3 Pa while O_2, with a pressure in the range of $(2 \div 5) \times 10^{-2}$ Pa, was the reactive gas. As expected, the oxygen partial pressure was seen to play a fundamental role on the real stoichiometry of the sputtered oxide film. Fig. 1 shows the behavior of the deposition rate (DR) of the Sn-O system as a function of the O_2 partial pressure, $P(O_2)$, keeping all other deposition parameters fixed.
It is clear that up to $P(O_2) = 2 \times 10^{-2}$ Pa the system is in the so-called metallic regime, characterized by the high-rate deposition (10 Å/s) of a quasi-metallic Sn film, while $P(O_2)$ above 5×10^{-2} Pa implies the low-rate deposition (0.4 Å/s) of a stoichiometric, SnO_2 film. Both these conditions are

not suitable for the deposition of the Sn-rich oxide film required for the diffusion process of the Sn atoms.

As a consequence, the appropriate working window of the oxygen pressure is in the $(3 \div 4) \times 10^{-2}$ Pa range. In particular, when the deposition rate is greater than 2 Å/s ($P(O_2) < 3.5 \times 10^{-2}$ Pa) a brownish film, formed by (SnO+Sn), is obtained. On the contrary, when the rate is 2 Å/s, a nearly stoichiometric SnO_2 ($SnO_{(2-x)}$) transparent film is obtained. Both these oxide films were tested as tin reservoir for the diffusion experiments. Specimens constituted of the sapphire substrate covered with ε-Ga_2O_3 + (SnO+Sn) or with ε-Ga_2O_3 + $SnO_{(2-x)}$ were introduced in an evacuated (10^{-4} Pa) quartz ampoule, then annealed in a muffle oven at a temperature of 600 °C for 4 hours. The temperature increase, up to 600 °C and the descent to RT were symmetric and determined by a 5 °C/min ramp. After the thermal process, the samples were chemically etched in the same way described above, in order to remove the residual tin-based oxide and get a clean ε-Ga_2O_3 surface.

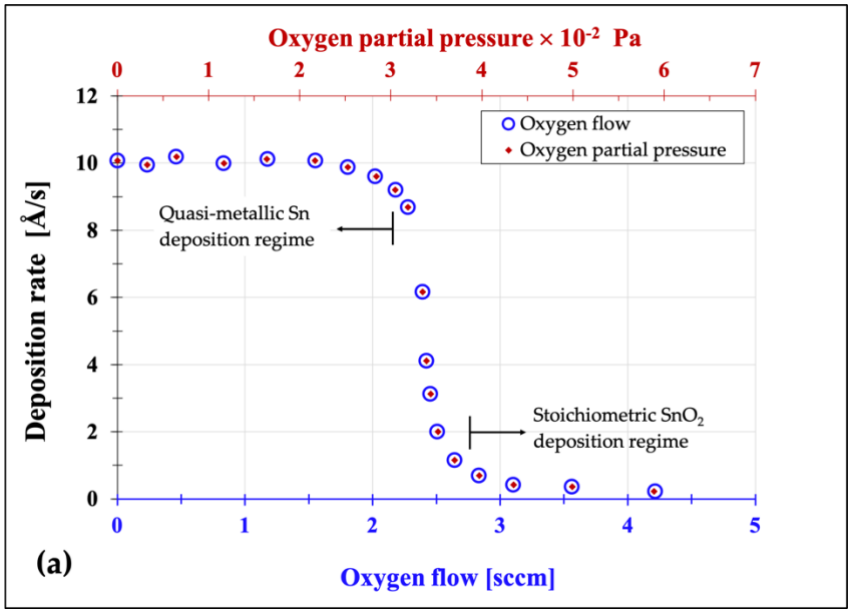

Figure 1: Deposition rate of the Sn-based oxide film as a function of the oxygen partial pressure (or oxygen flow rate) at fixed reactive sputtering parameters.

In order to know the chemical composition of the tin oxide film before and after the high temperature treatment, Rutherford Back-scattering Spectroscopy (RBS) and Raman spectroscopy were performed.

Raman spectra were recorded at the 473.1 nm line emission of a doubled Nd:YAG diode pumped laser in a nearly backscattered geometry with a HORIBA-Jobin Yvon LabRam confocal micro-spectrometer (300 mm focal length spectrograph) equipped with an integrated Olympus BX40 microscope, with 4x, 10x, 50x Ultra Long Working Distance (ULWD) and 100x objectives. The spectral resolution was about 3 cm^{-1}. Before measurements, the system was calibrated using the 520.6 cm^{-1} Raman peak of silicon. Data analysis was performed by LabSpec 5 built-in software. The (S)TEM investigations were carried out in an aberration corrected THEMIS microscope at 200 keV. For the EDS mapping a Super-X detector was used. The cross-sectional TEM samples were prepared by FIB sample preparation technique.

RBS analysis was performed in a scattering chamber with a two-axis goniometer connected to a 5 MV Van de Graaff accelerator operating at the Wigner Research Centre for Physics in Budapest. The 2 MeV $4He^+$ analyzing ion beam was collimated with two sets of four-sector slits to the dimensions of 0.5×0.5 mm^2, while the beam divergence was kept below 0.06°. The beam current

was measured by a transmission Faraday cup. In the scattering chamber the vacuum was about 1×10^{-4} Pa. To reduce the hydrocarbon deposition, liquid N_2 cooled traps were used along the beam path and around the wall of the chamber. Back-scattered He^+ ions were detected using an ORTEC surface barrier detector mounted in Cornell geometry at scattering angle $\Theta = 165°$. The energy resolution of the detection system was 15 keV. Spectra were recorded at sample tilt angles of 7° and 60°, respectively. In all experiments, axial and planar channeling of the He^+ in the gallium oxide film was avoided. The measured RBS spectra were evaluated with the SIMNRA [20] spectrum simulation code.

Some samples were characterized by ToF-SIMS as well. Depth profiles were obtained by a dual beam ION-TOF IV instrument (ION-TOF GmbH) using Cs^+ ions with energy of 2 keV with a current of 89.3 nA for sputtering an area of 300 μm × 300 μm and Ga^+ ions with energy of 25 keV, current 2.0 pA for the analysis of a 100 μm x 100 μm area within the sputtered crater; secondary ions were collected in negative polarity. These measurements were very useful to learn how deep the Sn atoms penetrated inside the ε-Ga_2O_3 film and their concentration profile. Collected data were first normalized to the Ga and carefully analyzed to avoid mass interferences without compromising detection limit. In particular, among the 10 natural isotopes of Sn, the most abundant are ^{120}Sn (32.58%), ^{118}Sn (24.22%) and ^{116}Sn (14.54%), only ^{116}Sn was unaffected by mass interference, as carefully checked through the mass peak inspection directly in the mass spectra during the depth profiling acquisition; thus, we consider ^{116}Sn a clean signature of the presence and localization of Sn into the films. Further, to get rid of any contribution from the background, we normalized the recorded ^{116}Sn intensity with the value of the intensity at the same mass spectra position for an undoped sample, considering the ratio I/I_0, where I is the intensity of the ^{116}Sn for the doped sample and I_0 is the intensity recorded on the undoped sample. Furthermore, for the calculation of the intensity ratios, we considered each intensity far from the surface, i.e. inside the ε-Ga_2O_3 layer and averaged the intensity collected over intervals of sputtering time.

After the deposition of ohmic contacts on the corners of square samples of Sn-doped ε-Ga_2O_3 epilayers [21], Hall effect investigation was performed in order to get information about the electrical activity of the Sn-diffused atoms. The van der Pauw method was applied, with a Keithley Hall-measurement setup. The data were collected in the 10-300 K temperature range, in vacuum and dark, and applying a magnetic field of 0.8 T for the detection of the Hall voltage.

3. Results and discussion

As already mentioned, due to its low melting point, metallic tin is not suitable for high temperature diffusion process. A specific deposition method by reactive sputtering in an oxidizing atmosphere starting with Sn metallic target, was developed to get a suitable tin reservoir for high-temperature diffusion. By changing $P(O_2)$, (SnO+Sn) or $SnO_{(2-x)}$ films were easily obtained.

When a DR > 2 Å/s was chosen for the reactive sputtering deposition, a (SnO+Sn) film is formed on top of the ε-Ga_2O_3 layer, while for DR = 2 Å/s the film resulted to be essentially SnO_2. Raman investigations confirm these results (see Fig. 2), although a precise determination of film composition, i.e. deviation from the perfect stoichiometry was not possible.

In Fig. 2a, the Raman peak of SnO at 210 cm^{-1} is observed in the spectrum, along with the signals from the sapphire substrate. Conversely, when DR = 2 Å/s a SnO_2 film is obtained, as confirmed from the SnO_2 Raman contributions in the spectrum of Fig. 2b [22].

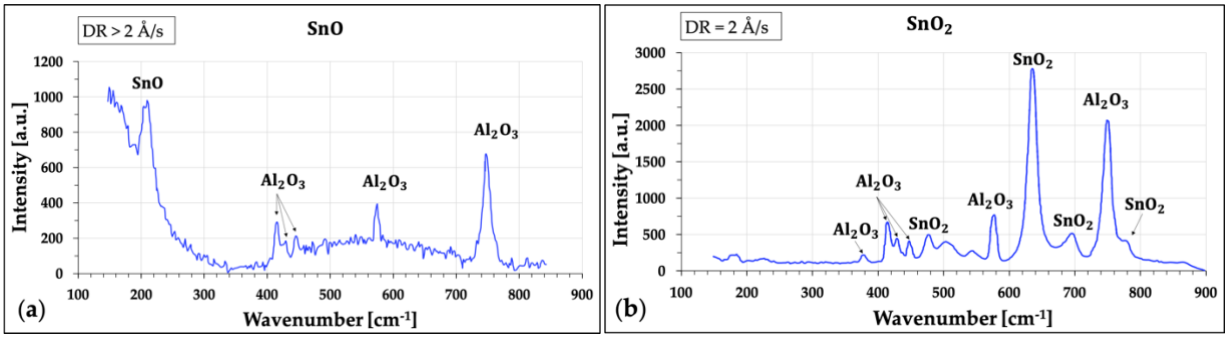

Figure 2: Raman spectra taken on as-deposited (SnO+Sn) and $SnO_{(2-x)}$ doping films deposited on top of the ε-Ga_2O_3 epilayer at fixed reactive sputtering parameters but with different oxygen partial pressures. (**a**) when DR > 2 Å/s and $P(O_2) < 3.5 \times 10^{-2}$ Pa a SnO film is obtained; (**b**) DR = 2 Å/s and $P(O_2) = 3.5 \times 10^{-2}$ Pa are effective to obtain a SnO_2 film. Sn-excess or O-deficiency in spectra (**a**) and (**b**), respectively, is below the detection threshold of the instrumentation.

An interpretation for this experimental evidence considers that the Sn excess in the $SnO_{(2-x)}$ is free to migrate into the Ga_2O_3 film while keeping a sharp interface between the two layers; i.e. maintaining a stable composition of both epitaxial layer and sputtered overlayer. On the other hand, SnO or (SnO+Sn) films proved to be unable to provide the desired Sn doping, probably because they "sucked" oxygen from the Ga_2O_3 film giving rise to a thin ternary $SnGaO_x$ barrier at the interface that impedes the further migration of Sn into Ga_2O_3. This mechanism was investigated by (S)TEM and Rutherford back-scattering in order to study the film microstructure and its composition. The TEM analysis was carried out on a 700 nm thick ε-Ga_2O_3 film with an overlaying 50 nm thick (SnO+Sn) film annealed in vacuum for four hours. HAADF image showed that the tin oxide was polycrystalline (see Fig. 3).

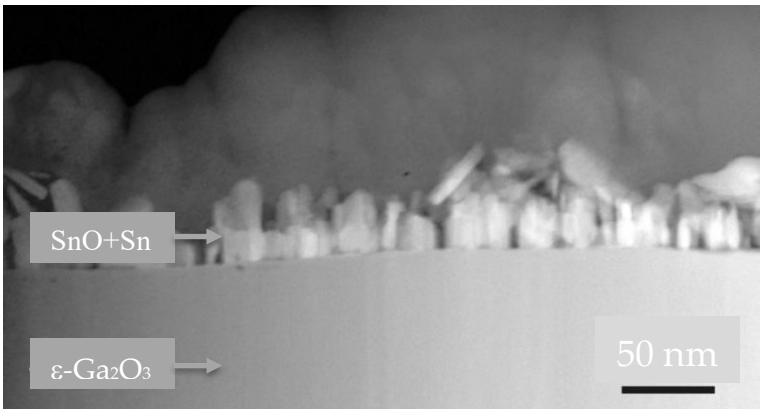

Figure 3: HAADF image of the (SnO+Sn) layer on the top of the Ga_2O_3 layer after annealing. This layer is composed of tiny grains and seems to be textured (see text for details).

A more detailed analysis of the (SnO+Sn) film, including fast Fourier transform (FFT), revealed that the layer contains SnO_2 inclusions close to the Ga_2O_3 interface (see Fig. 4 (a,b)) embedded in a SnO matrix. Considering that the layer was Sn rich, this finding confirms that oxygen escaped from Ga_2O_3 during annealing and led to formation of SnO_2 grains.
As a matter of fact, when (SnO+Sn), with composition close to SnO and far from SnO_2 was used, Sn was not effectively incorporated into the Ga_2O_3 layer. Of course, some Sn atoms could have penetrated into the Ga_2O_3 but their concentration was definitely below the detection limit of EDX

so that the boundary between tin and gallium oxide appeared to be very sharp, as shown in Fig. 4(c).

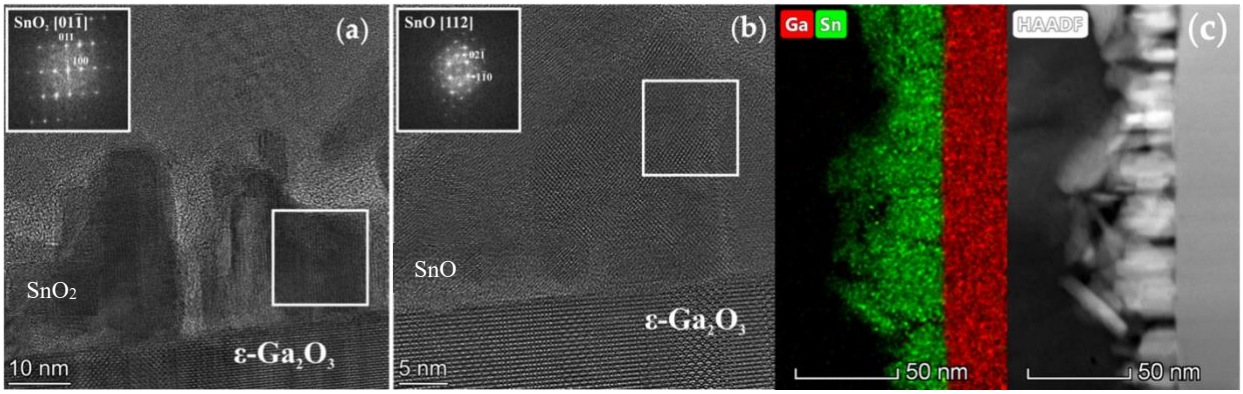

Figure 4: HRTEM image from the (SnO+Sn) layer. It is polycrystalline and textured; most of the layer is not epitaxial. (**a**) FFT from the marked area shows an epitaxial grain of rutile-type SnO_2; ((011)SnO_2 || (001)ε-Ga_2O_3 and (100)SnO_2 || (100)ε-Ga_2O_3). (**b**) FFT from the marked area shows a large epitaxial grain of SnO on the top of the Ga_2O_3; ((02-1)SnO || (001)ε-Ga_2O_3). (**c**) Z-contrast HAADF image from the layer with EDX Ga and Sn map.

At the same time, the Ga atoms made free at the interface after oxygen outdiffusion from Ga_2O_3 may bind with tin and oxygen and give rise to a thin ternary alloy that seems to act as stopping layer, preventing further diffusion of tin towards gallium oxide and, vice versa, of gallium towards tin oxide. It must be noted that this sample was only slightly conductive after the (SnO+Sn) coating-and-anneal treatment.

Rutherford Backscattering Spectroscopy was attempted in order to confirm this interpretation. Fig. 5(a,b) shows the measured RBS spectra on two different samples, and corresponding SIMNRA simulations made in two different ways. In Fig. 5(a) the experimental data are fitted considering a smooth planar structure for the (SnO+Sn) layer (sample 389 Sn4 in Tab 2). In this case, a good fit of the spectra is obtained assuming the formation of a ternary compound Sn-Ga-O of variable composition. In particular, considering four sublayers of same thickness with compositions: 14 nm $Sn_{0.8}Ga_{0.2}O_2$ - 14 nm $Sn_{0.73}Ga_{0.27}O_2$ - 14 nm $Sn_{0.4}Ga_{0.6}O_2$ - 14 nm $Sn_{0.25}Ga_{0.75}O_2$ / 720 nm Ga_2O_3, from upper free surface down to the substrate. In other words, the interface between the MOVPE film and the sputtered one was no longer abrupt. This is true for both 7° and 60° sample tilt angles (only the 7° measurements are reported in Fig. 5).

A completely different picture was considered in order to get the fitting of Fig. 5(b). Here, the roughness of the (SnO+Sn) layer structure, estimated from the HAADF in Fig. 3, was taken into account. For this fitting, the upper tin oxide layer was supposed to be uniform in composition but with a roughness of about 42 nm; see the simulation parameters in Table 1. We have to note this type of roughness-driven fitting is in good agreement with the experimental data only when one considers the upper oxide-based layer as largely oxygen-rich ($SnO_{2.7}$), which however contradicts the deposition parameters. Furthermore, the layer/substrate interface was considered to be sharp, without significant concentration gradients for Ga and Sn, in agreement with Z-contrast HAADF experiments. All in all, the real sample structure and composition are probably intermediate between the two models described in Fig. 5(a) and (b), that means a certain degree of roughness combined with a composition gradient.

RBS experiments were then repeated on another sample (478 Sn1) capped with a weakly oxygen-poor tin dioxide ($SnO_{(2-X)}$) layer. The sample for RBS was cut after annealing, without removing the tin dioxide capping and measured in the same conditions of those described above. Electrical measurements were carried out on another portion of the treated structure, after etching away

the residual tin dioxide, and showed that the nominally undoped Ga_2O_3 film exhibited high conductivity after the coating-and-anneal process. The RBS spectrum of this sample is shown in Fig. 5(c). Microscopic observation showed that the $SnO_{(2-X)}$ layer was smooth and flat, therefore the simulation was carried out without introducing any roughness. A convincing fitting was obtained by considering a uniform capping layer (~ 65 nm thick) of composition $SnO_{2.2}$. It is to be noted that the oxygen content is somewhat higher than the initial one, which confirms a diffusion of Sn towards the Ga_2O_3 film, corresponding to the oxygen enrichment, although a certain migration of oxygen from the epilayer towards the cap cannot be excluded. In any case, oxygen outdiffusion from Ga_2O_3 was surely much less consistent than in the case of (SnO+Sn) capping. Consequently, less Ga atoms are freed, and the intermediate Sn-Ga-O blocking layer does not form. These considerations again confirm the crucial role played by the composition of the Sn-O capping layer.

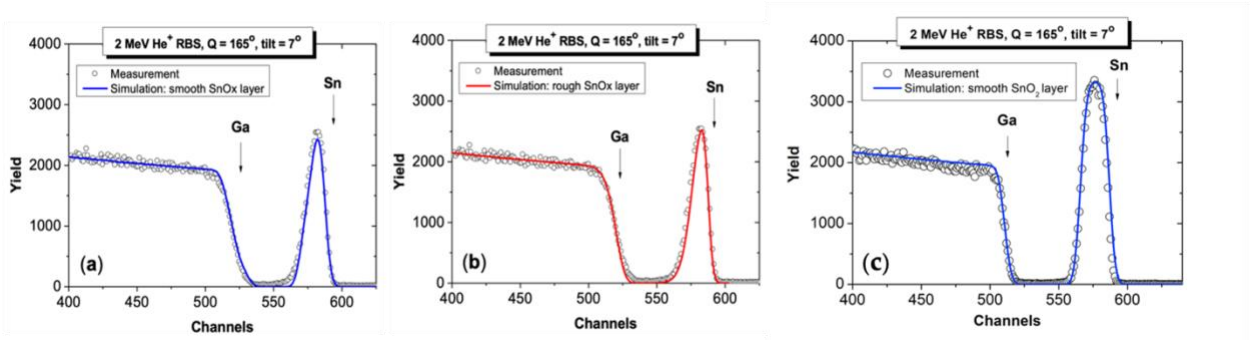

Figure 5: 2 MeV He^+ RBS spectrum for samples 389 Sn4 (**a,b**) and 478 Sn1 (**c**), taken at a tilt angle of 7°. The arrows indicate the spectrum edges for different components. Solid line shows the result of SIMNRA simulation considering: (**a**) smooth structure and variable composition of the oxide capping layer, (**b**) rough surface and uniform composition of the largely O-rich capping layer. Note that this sample was only slightly conductive. (**c**) refers to 478 Sn1 sample, which was converted from nominally-undoped resistive to *n*-type conductive; SIMNRA simulation was very satisfactory taking a slightly O-rich smooth $SnO_{(2-x)}$ capping layer. See text for more details.

Sample	Capping layer			Ga_2O_3
	Thickness [nm]	Composition	Roughness (FWHM) [nm]	Thickness [nm]
389 Sn4	44	$SnO_{2.7}$	42	730
478 Sn1	65	$SnO_{2.2}$	===	400

Table 1: Parameters used in SIMNRA simulations of RBS spectra of the 389 Sn4 and 478 Sn1 samples.

In Table 2, the behavior of different ε-Ga_2O_3 samples, subjected to different diffusion processes is summarized. In particular, sample #226 C2 exhibits a RT resistivity ρ = 120 Ω·cm, a too high value if compared with typical resistivity of Sn-doped β-Ga_2O_3 [23, 24] or Si-doped ε-Ga_2O_3 [17].

sample	Thickness (Ga_2O_3) [nm]	$P(O_2)$ x 10^{-2} [Pa]	$\Phi(O_2)$ [sccm]	Tin-oxide thickness [nm]	T_{dep} [°C]	T_{ann} [°C]	$Time_{ann}$ [min]	RT-resistivity [Ω·cm]
# 226 C2	450	2.9	2	35	600	600	240	120
# 317 Sn1	400	3.4	2.4	35	600	600	240	7.5
# 317 Sn2	400	3.4	2.4	30	RT	600	240	8.7
# 317 Sn3	350	3.4	2.4	40	RT	600	600	6.8
# 321 Sn4	300	3.5	2.5	50	RT	600	120	14
# 368 Sn4	300	3.4	2.4	100	RT	600	240	8.5
# 369 Sn5	300	3.4	2.4	50	RT	600	240	6.8
# 421 Sn3	300	3.5	2.5	50	RT	630	240	3.6
# 421 Sn2	300	3.5	2.5	50	RT	600	240	1.3
# 389 Sn4	700	2.7	1.8	50+50	RT	600	240+240	60
# 478 Sn1	400	3.5	2.5	50	RT	600	240	2.4

Table 2: Information related to investigated samples; during their preparation only one parameter was changed, keeping all the others fixed. Only for #226 C2 and #389 Sn4 samples the doping layer was (SnO+Sn); all the other samples were doped by means of $SnO_{(2-x)}$ films.

Differences and similarities, found between samples, are listed below, by comparing the parameters used for their preparation.

- *Oxygen partial pressure:* #226 C2 and 317 Sn1 samples exhibit a RT resistivity of 120 Ω·cm and 7.5 Ω·cm respectively. The difference between these two samples is the oxygen partial pressure used during the reactive sputtering deposition: under a pressure of 2×10^{-2} Pa a (SnO+Sn) layer is deposited (#226 C2), which is much less effective as dopant layer than the $SnO_{(2-x)}$ film (317 Sn1) deposited with an oxygen partial pressure of 3.4×10^{-2} Pa.
- *Deposition temperature*: #317 Sn1 and #317 Sn2 samples are characterized by the deposition of the $SnO_{(2-x)}$ film at a temperature of 600 °C and RT respectively. These samples exhibit RT resistivity of 7.5 Ω·cm ad 8.7 Ω·cm respectively, demonstrating a negligible dependence of the resistivity, i.e. Sn diffusion, on the $SnO_{(2-x)}$ film deposition temperature.
- *Doping process time*: #317 Sn2, #317 Sn3 and #321 Sn4 were annealed in vacuum at a temperature of 600 °C for 240 min, 600 min and 120 min respectively. For the first two samples, RT resistivity values are similar despite very different annealing times, suggesting that all the Sn free atoms, coming from the $SnO_{(2-x)}$ film, are effectively diffused

into the Ga_2O_3 layer after 240 min, and an additional stay at high temperature is not beneficial for further diffusion of Sn atoms, while 120 min are not enough for the complete exploitation of the Sn excess in the sputtered overlayer.

- *Thickness of the $SnO_{(2-x)}$ film*: # 317 Sn3 and # 368 Sn4 are samples with different thickness of the $SnO_{(2-x)}$ capping layer. No considerable difference in RT resistivity was noted, when a thickness of 40 nm or 100 nm of the $SnO_{(2-x)}$ film was used.
- *Annealing temperature*: #369 Sn5 and #421 Sn3 samples were annealed at 600 °C and 630 °C respectively, but negligible difference in RT resistivity was observed. As *n*-type conductivity depends on the number of Sn atoms on Ga-sites, via successive occupancy of the Ga-vacancies, it can be concluded that at higher temperature, Sn diffusion is probably faster, but it does not improve the doping, which is essentially limited by the available Ga vacancy concentration.
- *RBS and (S)TEM analysis:* #389 Sn4 sample was prepared by using two complete doping cycles with (SnO+Sn) as capping layer. #478 Sn1 sample was prepared using the optimized $SnO_{(2-x)}$-based sequence. These samples were analyzed without having made any chemical etching of the doping layer in order to investigate the (SnO+Sn) or $SnO_{(2-x)}$ films and the interface with Ga_2O_3 by means of RBS and (S)TEM analysis.
- *The optimized process*: considering all the above observations, an optimized process was developed. As an example, see the process parameters reported in Tab. 2 for sample #421 Sn2, whose RT resistivity is probably the lowest ever reported for Sn-doped ε-Ga_2O_3.

Each diffusive phenomenon is characterized by a concentration gradient and by the solubility limit of the diffusing species, which depends on temperature. In the present case, being the temperature fixed at 600 ° C, a question arises: when does the diffusion process go to completion? Namely, is the whole ε-Ga_2O_3 film uniformly doped or can we expect a Sn concentration profile across the Ga_2O_3 epilayer? For answering, some diffusion experiments on a 2.3 μm thick ε-Ga_2O_3 film were performed and the results were summarized in Table 3.

sample	Thickness (Ga_2O_3) [nm]	D.R. [Å/s]	$\Phi(O_2)$ [sccm]	Tin-oxide thickness [nm]	T_{ann} [°C]	$Time_{ann}$ [min]	RT-resistivity [Ω·cm]
# 425 Sn1a	2300	2	2.5	50	600	240	34.2
# 425 Sn2a	2300	2	2.5	50+50	600	240+240	12.0
# 425 Sn3a	2300	2	2.5	50+50+50	600	240+240+240	8.6
# 425 Sn4a	2300	2	2.5	50+50+50+50	600	240+240+240+240	1.3

Table 3: Four equivalent specimens, coming from the same ε-Ga_2O_3 epilayer (#425), were submitted to subsequent diffusion cycles, under the same conditions. One cycle consisted of 50 nm thick $SnO_{(2-x)}$ film deposited on top ε-Ga_2O_3, followed by annealing at 600 °C for 4h and then F-N etching in order to remove the residual $SnO_{(2-x)}$. The sample 1a was treated with one cycle only, the sample 2a was treated with a sequence of two complete cycles, the 3a with three sequential complete cycles and, finally, the 4a was treated with four complete doping cycles. For each sample, the electrical measurements were performed only after its complete doping sequence.

From the RT resistivity values, with only one doping cycle, the concentration of Sn atoms into the ε-Ga_2O_3 lattice is not maximized and diffusion does not reach a saturation level. Diffusion of Sn atoms in these thick films goes to saturation only after 4 doping cycles. After multiple processing, the resistivity of thick epilayers reaches the value generally obtained in thinner ε-Ga_2O_3 films.
This aspect is well corroborated by ToF-SIMS analysis, where a trend of progressive increment of the I/I_0 intensity ratio for the mass ^{116}Sn is calculated, as shown in Fig. 6(a). In the figure, sample #355 Ud1 is an undoped sample used as reference. It is worth noting that, considering the samples treated only once and the sample subjected to 3 cycles, the I/I_0 ratio changes from 2.7 to 11, i.e. of about a factor of 4, and concomitantly the resistivity decreases from 34.2 to 8.6 Ω·cm, by a factor of 4. This is a strong indication that the measured changes in resistivity are correlated with the amount of Sn atoms subsequently diffused into the ε-Ga_2O_3 film. In Fig. 6(b) samples labelled 260 Sn1, 256 Sn1 and 226 Sn2 were treated with an (SnO+Sn) doping layer, while the 355 Sn1 and 421 Sn7 were annealed under the $SnO_{(2-x)}$ film. Also in this case, even considering that the tin diffusion process was not yet fully optimized, an increasing trend of the I/I_0 ratio is observed when passing from (SnO+Sn) to $SnO_{(2-x)}$ as doping layer.
Further, when considering any sub-set of samples listed in Table 2, the ^{116}Sn intensity ratio is seen to change only slightly, being in the mid-range value around 4 - 5.5. The trend of this ratio is compatible with that one of the measured resistivity values; in particular, the I/I_0 values confirms the effective diffusion of Sn atoms inside the ε-Ga_2O_3 film. The different treatment conditions do not affect much the diffusion of Sn atoms inside the ε-Ga_2O_3 layer, provided that the right composition for the Sn-containing capping is chosen.

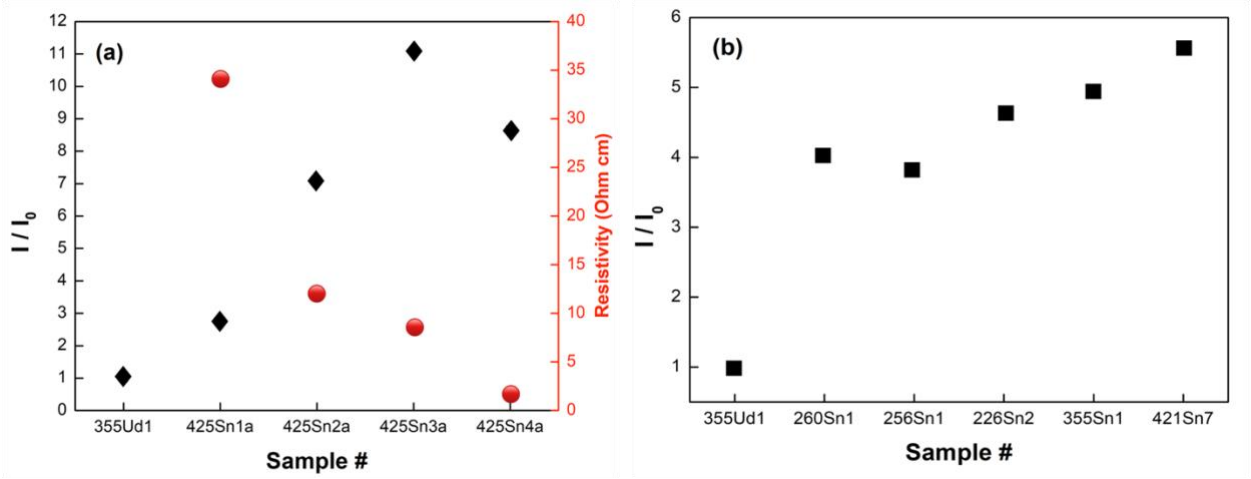

Figure 6: Intensity ratio for mass ^{116}Sn as recorded during ToF-SIMS depth profiling inside ε-Ga_2O_3 layers. (**a**) together with the resistivity for samples listed in Table 3; (**b**) for samples treated as some of those reported in Table 2. In both graphs, sample #355 Ud1 is an undoped sample used as reference (see text in Experimental section for details).

Our Tof-SIMS and TEM observations actually point to the following mechanism: in case of strong oxygen deficiency (layer (SnO+Sn)), oxygen atoms migrate from the ε-Ga_2O_3 epilayer to the overlying sputtered layer upon thermal anneal, hence giving rise to SnO_2 islands in the upper layer and leaving a thin Ga-rich region close to the interface, which ultimately forms a ternary $SnGaO_x$ layer. The latter acts as barrier against further species interdiffusion so that the composition of the two layers remains constant after a certain transition period (dictated by oxygen outdiffusion).
On the contrary, a little oxygen deficiency (that we have indicated as $SnO_{(2-x)}$) makes the continuous migration of "free" Sn atoms from the capping into the underlying Ga_2O_3 epitaxial film possible.

Summarizing, it seems that an excessive Sn content in the SnO compound directly in contact with the ε-Ga_2O_3 surface, causes the formation of an intermixing layer, limiting the availability of Sn atoms for further diffusion. It should be considered that SnO is not a stable phase in presence of oxygen, exhibiting a natural tendency to transform in SnO_2. The difference in the enthalpies of formation between SnO (ΔH^0_f = -281 kJm^{-1}) and SnO_2 (ΔH^0_f = -577 kJm^{-1}) justifies the formation of the latter at the expense of the former, in presence of oxygen excess. This may actually occur due to oxygen outdiffusion from ε-Ga_2O_3 towards a (SnO+Sn) coating. Removing oxygen from the ε-Ga_2O_3 layers, also makes some Ga atoms free, which promotes the formation of a mixed ternary compound Ga-Sn-O. With this compound at the interface, the possibility that other tin atoms may diffuse within the underlying ε-Ga_2O_3 is lost, since the mixed compound may act as a buffer layer against further diffusion into ε-Ga_2O_3. This can explain the minor level of doping achieved by using Sn-rich (SnO+Sn) film as a supplier of tin atoms. On the other hand, a DR = 2 Å/s, obtained with a $P(O_2)$ fine-tuning during sputtering, is effective for the deposition of an oxygen-poor $SnO_{(2-x)}$ film (see Fig. 2(b)), which proved to be the most suitable coating for carrying out the diffusive process of tin atoms into the ε-Ga_2O_3 layer.

Transport measurements as a function of temperature were performed on the Sn-doped samples to investigate their electrical properties. A reduction of several orders of magnitude in the resistivity of diffused samples with respect to undoped films is observed. For the latter, values higher than 10^7 Ω·cm were typically measured. The result indicates that an effective doping process occurred and, although the low mobility permitted to detect the Hall voltage only in few cases, the *n*-type conductivity of the layers was confirmed [24]. The resistivity was measurable in all samples in a wide temperature range, and double-slope linear trends were always observed when the natural logarithm of the resistivity was plotted vs $T^{1/4}$ (*Mott plot*). Such a behavior is shown in Fig. 7(a,b) and it basically reproduces what was found in Si-doped *n*-type ε-Ga_2O_3 samples [17]. A linear behavior of the resistivity in a similar plot is consistent with the Mott law, applicable in case of variable range hopping (VRH) transport mechanism:

$$\rho(T) = \rho_0 \exp\left[(T_0/T)^{1/4}\right] \qquad (1)$$

where the T_0 temperature is defined as: $T_0 = C/(\xi^3 g(\mu) K_B)$, with K_B the Boltzmann constant, $g(\mu)$ the density of the energy states around of the Fermi level, ξ the localization radius, which is the spatial extent of the wave-function of an electron localized at a single site. The proportionality constant C is an empiric dimensionless parameter depending on the network of hopping sites. In Equation (1) the pre-exponential term ρ_0 represents the resistivity at infinite temperature. Further details on the model are reported in Refs. [17, 25].

From Equation (1), the slope of the linear trend in a *Mott plot* equals the quantity $T_0^{1/4}$, which is related to $g(\mu)$. Typical values of the localization radius are of the order of a few nm and a value $C = 8^3/9\pi$ can be assumed for the empirical parameter, as for a 3D non-interacting electron gas and randomly distributed hopping sites. Therefore, from the slopes of the data of Fig. 7 the density of the defects involved in the hopping conduction can be estimated.

Two well evident linear traits are visible in the *Mott plot* for all measured Sn-diffused samples. The inspection of Fig. 7 permits to conclude that the resistivity decrease, from sample to sample, corresponding to higher doping, is always related to a reduction of the slopes in the *Mott plot*, indicating a $g(\mu)$ increases, as well as an increase of the hopping-site density. Doping level and density of hopping sites are then correlated, and the slopes of the linear segments give a rough evaluation of the doping levels. It is worth noting that samples #421 Sn2 and #425 Sn4a, showing comparable RT resistivity, exhibit very similar slopes of the *Mott plot* despite the different diffusion methods. Certainly, compensation due to acceptor defects or unintentional acceptor

impurities is also expected to play a role in the transport mechanism. Evidence of the Sn penetration in the whole layer thickness given by ToF-SIMS investigation and the similarity with the resistivity behavior observed in Si doped samples (discussed in Ref. [17]) strongly support the identification of Sn as substitutional impurity, which forms an impurity band within which carriers move by hopping.

In Fig. 7, the low- (LT) and high-T (HT) slopes are reported for the lowest (Fig. 7(a)) and the heaviest (Fig. 7(b)) doped samples: the corresponding doping levels, derived by the LT and HT slopes of the two linear traits, increase of about one order of magnitude, within the range (10^{17}÷10^{18}) cm^{-3}. These values are consistent with the Hall density. Then, the RT resistivity difference of an order of magnitude between the lowest and the highest doped samples (see Table 2) indicates that the mobility must be of few $cm^2/V{\cdot}s$ in any case.

The double slope behavior of the Mott plots was previously encountered in Si-doped ε-Ga_2O_3 [25]. An extensive EPR investigation in that case confirmed the occurrence of variable range hopping (VRH) transport involving Si-donors.

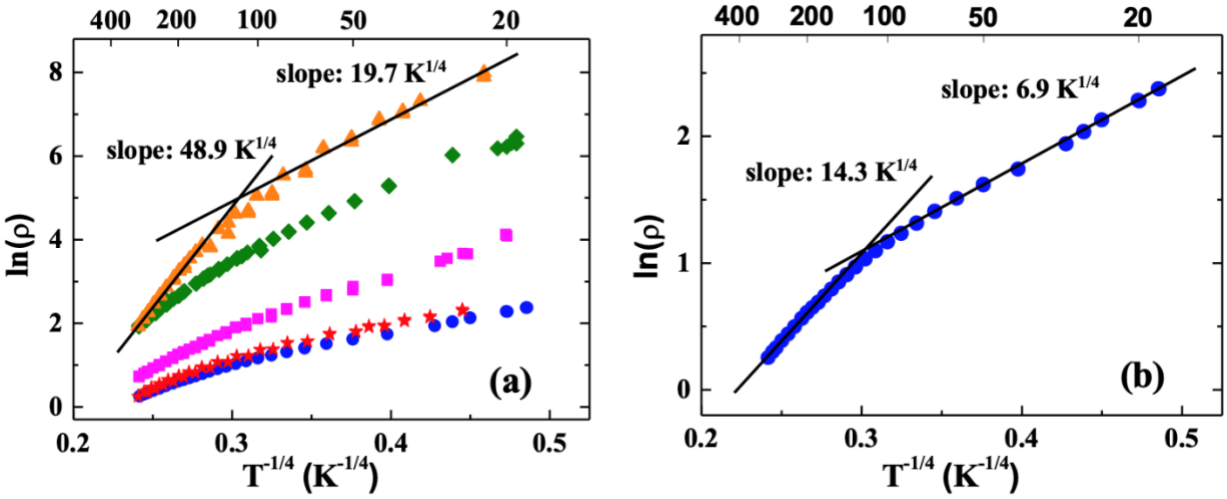

Figure 7: (**a**) Natural logarithm of the resistivity data (expressed in Ω·cm) vs. $T^{-1/4}$ (Mott plot) of some samples of Table 2 and Table 3 (orange triangles: #321 Sn4; green rhombi: #317 Sn1; magenta squares: #369 Sn5; blue circles: #421 Sn2); red stars: #425 Sn4a. (**b**) Enlargement of the data of #421 Sn2, to better highlight the broken-line trend of the Mott plot. In both the figures the continuous lines, overlapped to the data of either the most and the less Sn-doped samples, represent the linear fits of the low-T and high-T data, having the nearby indicated slopes.

4. Conclusion

A novel method for *n*-type doping ε-Ga_2O_3 films was developed. It includes encapsulation of the original ε-Ga_2O_3 epilayer by a sputtered $SnO_{(2-x)}$ film and subsequent annealing at 600°C in vacuum for at least 4 hours. The diffusion process goes to completion within this time only if the ε-Ga_2O_3 film is relatively thin (200-300 nm) while for thicker epilayers the entire process must be repeated in order to get diffusion saturation. It is seen that the sputtering deposition rate, i.e. stoichiometry of the $SnO_{(2-x)}$ overlayer, is a most crucial factor: only O-poor SnO_2 is effective in promoting the diffusion of its Sn excess in the underlying ε-Ga_2O_3 epilayer. By applying different investigation techniques, we came to the somewhat surprising conclusion that when the encapsulating layer contains much free Sn, a certain amount of oxygen may be drained from ε-Ga_2O_3, which produces some SnO_2 domains within the capping and frees some Ga atoms at the

interface. The latter give rise to a thin ternary $SnGaO_x$ alloy at the interface that blocks the further Sn diffusion into the ε-Ga_2O_3. The interface between Ga_2O_3 and the Sn-based oxide thus plays a fundamental role during the diffusion of Sn atoms depending on the involved phase diagram and the chemical reactivity of the present atomic species.
This diffusion method has been successfully applied to *n*-doping of the ε-Ga_2O_3 films routinely grown by MOVPE by our research team in Parma. Nominally-undoped as-grown films with resistivity of about 10^7 Ω·cm exhibited a resistivity of (1÷10) Ω·cm after the diffusion process.
Electrical characterization suggested that the electronic transport takes place via variable-range hopping.

Acknowledgments

Exchange of samples and researchers' visits between Italy and Hungary were possible in the framework of the CNR and MTA bilateral scientific agreement.
The authors acknowledge Prof. Danilo Bersani, Prof. Pier Paolo Lottici and Prof. Davide Orsi of the University of Parma for the availability of the Raman spectroscopy Laboratory.

References

[1] S. J. Pearton, J. Yang, P. H. Cary IV, F. Ren, J. Kim, M. J. Tadjer and M. A. Mastro, "A review of Ga_2O_3 materials, processing, and devices," *Applied Physics Reviews,* vol. 5, p. 011301, 2018.

[2] M. F. Al-Kuhaili, M. A. Durrani and E. E. Khawaja, "Optical properties of gallium oxide films deposited by electron-beam evaporation," *Appl. Phys. Lett.,* vol. 83, p. 4533, 2003.

[3] R. Roy, V. G. Hill and E. F. Osborn, "Polymorphism of Ga_2O_3 and the System Ga_2O_3-H_2O," *J. Am. Chem. Soc. ,* vol. 74, no. 3, pp. 719-722, 1952.

[4] F. Alema, B. Hertog, O. Ledyaev, D. Volovik, G. Thoma, R. Miller, A. Osinsky, P. Mukhopadhyay, S. Bakhshi, H. Ali and W. V. Schoenfeld, "Solar blind photodetector based on epitaxial zinc doped Ga_2O_3 thin film," *Phys. Status Solidi A,* vol. 172, p. 1600688, 2017.

[5] K. D. Chabak, N. Moser, A. J. Green, D. E. Walker, S. Tetlak, E. Heller, A. Crespo, R. Fitch, J. P. McCandless, K. Leedy, M. Baldini, G. Wagner, Z. Galazka, X. Li and G. Jessen, "Enhancement-mode Ga_2O_3 wrap-gate fin field-effect transistors on native (100) β-Ga_2O_3 substrate with high breakdown voltage," *Appl. Phys. Lett.,* no. 109, p. 213501, 2016.

[6] M. Baldini, Z. Galazka and G. Wagner, "Recent progress in the growth of β-Ga_2O_3 for power electronics applications," *Materials Science in Semiconductor Processing,* vol. 78, pp. 132-146, 2018.

[7] A. Zunger, "Practical doping principles," *Appl. Phys. Lett. ,* vol. 83, p. 57, 2003.

[8] J. B. Varley, J. R. Weber, A. Janotti and C. G. Van de Walle, "Oxygen vacancies and donor impurities in β-Ga_2O_3," *Appl. Phys. Lett. ,* vol. 97, p. 142106, 2010.

[9] J. B. Varley, H. Peelaers, H. Janotti and C. G. van de Walle, "Hydrogenated cation vacancies in semiconducting oxides," *J. Phys.: Condens. Matter,* vol. 23, no. 33, p. 334212, 2011.

[10] T. Zacherle, P. C. Schmidt and M. Martin, "Ab initio calculations on the defect structure of β-Ga_2O_3," *Physical Review B,* vol. 87, p. 235206, 2013.

[11] F. A. Kröger, "Preparation, Purification, Crystal Growth And Phase Theory," in *The Chemistry of Imperfect Crystals, 2nd ed.*, Amsterdam, North-Holland, 1973, pp. K67-K68.

[12] J. E. N. Swallow, "Influence of Polymorphism on the Electronic Structure of Ga_2O_3," *arXiv:2005.13395 [cond-mat.mtrl-sci],* submitted May, 27 2020.

[13] M. Saleh, J. B. Varley, J. Jesenovec, A. Bhattacharyya, S. Krishnamoorthy, S. Swain and K. Lynn, "Degenerate doping in β-Ga_2O_3 single crystals through Hf-doping," *Semicond. Sci. Technol. 35 04LT01,* vol. 35, pp. 1-6, 2020.

[14] W. Zhou, C. Xia, Q. Sai and H. Zhang, "Controlling n-type conductivity of β-Ga_2O_3 by Nb doping," *Appl. Phys. Lett. ,* vol. 111, no. 24213, pp. 1-4, 2017.

[15] A. T. Neal, S. Mou, S. Rafique, H. Zhao, E. Ahmadi, J. S. Speck, K. T. Stevens, J. D. Blevins, D. B. Thomson, N. M. Kelson, D. Chabak and G. H. Jessen, "Donors and deep acceptors in β-Ga_2O_3," *Appl. Phys. Lett. 113, 062101 (2018);,* vol. 113, no. 062101, pp. 1-5, 2018.

[16] M. J. Tadjer, J. L. Lyons, N. Nepal, J. A. Freitas Jr., A. D. Koehler and G. M. Foster, "Theory and Characterization of Doping and Defects in β-Ga_2O_3," *ECS J. Solid State Sci. Technol.,* vol. 8, no. 7, pp. Q3187-Q3194, 2019.

[17] A. Parisini, A. Bosio, V. Montedoro, A. Gorreri, A. Lamperti, M. Bosi, G. Garulli, S. Vantaggio and R. Fornari, "Si and Sn doping of ε-Ga_2O_3 layers," *APL Materials WBO 2019,* vol. 7, no. 031114, pp. 1-5, 2019.

[18] F. Boschi, M. Bosi, T. Berzina, E. Buffagni, C. Ferrari e R. Fornari, «Hetero-epitaxy of ε-Ga_2O_3 layers by MOCVD and ALD,» *J. Crystal Growth ,* vol. 443, pp. 25-30, 2016.

[19] R. Fornari, M. Pavesi, V. Montedoro, D. M. F. Klimm, I. Cora, B. Pécz, F. Boschi, A. Parisini, A. Baraldi, C. Ferrari, E. Gombia and M. Bosi, "Thermal stability of ε- Ga_2O_3 polymorph," *Acta Materialia,* vol. 140, pp. 411-416, 2017.

[20] M. Mayer, "Improved physics in SIMNRA 7," *Nuclear Instruments and Methods in Physics Research Section B: Beam Interactions with Materials and Atoms,* vol. 332, pp. 176-180, 2014.

[21] A. Bosio, C. Borelli, A. Parisini, M. Pavesi, S. Vantaggio and R. Fornari, "A Metal-Oxide Contact to ε-Ga_2O_3 Epitaxial Films and Relevant Conduction Mechanism," *ECS Journal of Solid State Science and Technology,* vol. 9, no. 5, p. 055002, 2020.

[22] J. Geurts, S. Rau, W. Richter e F. J. Schmitte, «SnO films and their oxidation to SnO_2: Raman scattering, IR reflectivity and X-ray diffraction studies,» *Thin Solid Films,* vol. 121, n. 3, pp. 217-225, 1984.

[23] X. Du, Z. Li, C. Luan, W. Wang, M. Wang, X. Feng, H. Xiao and J. Ma, "Preparation and characterization of Sn-doped β-Ga_2O_3 homoepitaxial films by MOCVD," *J Mater Sci ,* vol. 50, pp. 3252-3257, 2015.

[24] D. Gogova, M. Schmidbauer and A. Kwasniewski, "Homo- and heteroepitaxial growth of Sn-doped β-Ga_2O_3 layers by MOVPE," *CrystEngComm,* vol. 17, p. 6744, 2015.

[25] H. J. von Bardeleben, J. L. Cantin, A. A. Parisini, A. Bosio and R. Fornari, "Conduction Mechanism and Shallow donor properties in Silicon doped ε-Ga_2O_3 thin films: an Electron Paramagnetic Resonance study," *Phys.Rev Mat.,* no. 3, pp. 084601-1 - 084601-8, 2019.

[26] M. Mulazzi, F. Reichmann, A. Becker, C. Wenger, A. Parisini, M. Bosi, V. Fiorentini and R. Fornari, "The electronic structure of ε-Ga_2O_3," *APL Material,* vol. 7, pp. 022522-1 - 022522-6, 2019.

[27] A. Parisini, A. Parisini and R. Nipoti, "Size effect on high temperature variable rangehopping in Al+ implanted 4H-SiC," *Journal of Physics: Condensed Matter,* vol. 29, pp. 035703-1 - 035703-14, 2016.